

A large interconnecting network within hybrid MEH-PPV/TiO₂ nanorod photovoltaic devices

Tsung-Wei Zeng¹, Yun-Yue Lin¹, Hsi-Hsing Lo¹,
Chun-Wei Chen^{1,4}, Cheng-Hsuan Chen², Sz-Chian Liou²,
Hong-Yun Huang² and Wei-Fang Su^{1,2,3,4}

¹ Department of Materials Science and Engineering, National Taiwan University, Taipei 106-17, Taiwan

² Center for Condensed Matter Sciences, National Taiwan University, Taipei 106, 106-17, Taiwan

³ Graduate Institute of Polymer Science and Engineering, National Taiwan University, Taipei 106-17, Taiwan

E-mail: chunwei@ntu.edu.tw and suwf@ntu.edu.tw

Received 24 June 2006, in final form 6 September 2006

Published 13 October 2006

Online at stacks.iop.org/Nano/17/5387

Abstract

This is a study of hybrid photovoltaic devices based on TiO₂ nanorods and poly[2-methoxy-5-(2'-ethyl-hexyloxy)-1,4-phenylene vinylene] (MEH-PPV). We use TiO₂ nanorods as the electron acceptors and conduction pathways. Here we describe how to develop a large interconnecting network within the photovoltaic device fabricated by inserting a layer of TiO₂ nanorods between the MEH-PPV:TiO₂ nanorod hybrid active layer and the aluminium electrode. The formation of a large interconnecting network provides better connectivity to the electrode, leading to a 2.5-fold improvement in external quantum efficiency as compared to the reference device without the TiO₂ nanorod layer. A power conversion efficiency of 2.2% under illumination at 565 nm and a maximum external quantum efficiency of 24% at 430 nm are achieved. A power conversion efficiency of 0.49% is obtained under Air Mass 1.5 illumination.

(Some figures in this article are in colour only in the electronic version)

1. Introduction

Conjugated polymers have great utility for fabrication of large area, physically flexible and low cost solar cells [1, 2]. A basic requirement for making efficient photovoltaic devices is that the free charge carriers produced upon photo-excitation of the photoactive material must be transported through the device to the electrode without recombining with oppositely charged carriers. Photovoltaic devices merely composed of conjugated polymers as the only active material have extremely low electron mobility and, thus, limited performance. Recent developments have shown that the use of interpenetrating electron donor–

acceptor heterojunctions such as polymer:fullerene [2–4], polymer:polymer [5] and polymer:nanocrystal [6–8] can yield highly efficient photovoltaic conversions. Electron acceptors have been intermixed at the nanometre scale with an organic semiconducting polymer to obtain high charge separation yield. Following electron transfer, both electron and hole must be transported to the electrode before back recombination can occur. However, in some cases, electron transport is limited by inefficient hopping along poorly formed conduction paths. Thus, an enhanced charge transport route is desirable to achieve efficient electron conduction. One-dimensional semiconductor nanorods are preferable for offering direct pathways for electric conduction [1, 9–11]. Huynh *et al* have produced high performance solar cells by combining CdSe nanorods with poly(3-hexylthiophene) (P3HT) [1].

⁴ Address for correspondence: Department of Materials Science and Engineering, National Taiwan University, Taipei 106-17, Taiwan.

Titanium dioxide (TiO₂) nanocrystals are promising as an electron accepting material in hybrid organic/inorganic photovoltaic device applications. Several different conjugated polymers have been used for the polymer: TiO₂ solar cells, such as poly[2-methoxy-5-(2'-ethyl-hexyloxy)-1,4-phenylene vinylene] (MEH-PPV) [12–15], MEH-PPV derivatives [16], poly[2-methoxy-5-(3',7'-dimethyloctyloxy)-1,4-phenylene vinylene] (MDMO-PPV) [17], P3HT [8, 18, 19] and water soluble polythiophene [20], etc. Many approaches produced devices by infiltrating polymers into sintered TiO₂ nanoporous thin film. Polymer:TiO₂ solar cells made from spin coating a blending of polymer–TiO₂ nanocrystals solution have been presented less often. The photoinduced charge transfer and recombination of TiO₂ nanorods and MEH-PPV hybrid has been reported, which suggests that the MEH-PPV:TiO₂ nanorod heterojunctions may be used as potential active material for photoconversion [21, 22]. In this study, we have fabricated an MEH-PPV:TiO₂ nanorod heterojunction photovoltaic device. The device performance is further enhanced by inserting a thin layer of TiO₂ nanorods between the photoactive material and the electrode for an efficient electron transport.

2. Experimental details

The controlled growth of high aspect ratio anatase titanium dioxide nanorods was accomplished by hydrolyzing titanium tetraisopropoxide according to the literature with some modifications [23]. Typically, oleic acid (120 g, Aldrich, 90%) was stirred vigorously at 120 °C for 1 h in a three-neck flask under Ar flow, then allowed to cool to 90 °C and maintained at this temperature. Titanium isopropoxide (17 mmol, Aldrich, 99.999%) was then added into the flask. After stirring for 5 min, trimethylamine-*N*-oxide dihydrate (34 mmol, ACROS, 98%) in 17 ml water was rapidly injected. Trimethylamine-*N*-oxide dihydrate was used as a catalyst for polycondensation. This reaction was continued for 9 h to have complete hydrolysis and crystallization. Subsequently, the TiO₂ nanorod product was obtained (4 nm in diameter, 20–40 nm in length). The nanorods were washed and precipitated by ethanol repeatedly to remove any residual surfactant. Finally, the TiO₂ nanorods were collected by centrifugation and then redispersed in chloroform or toluene.

The indium–tin–oxide (ITO)/poly(3,4-ethylenedioxythiophene)-poly(styrenesulfonate) (PEDOT:PSS)/MEH-PPV:TiO₂ nanorods/Al device was fabricated in the following manner. An ITO glass substrate with a sheet resistance of 15 Ω/square (Merck) was ultrasonically cleaned in a series of organic solvents (ethanol, methanol and acetone). A 60 nm thick layer of PEDOT:PSS (Aldrich) was spin-cast onto the ITO substrate; this was followed by baking at 100 °C for 10 min. TiO₂ nanorods in toluene and MEH-PPV (Aldrich, molecular weight 40 000–70 000 g mol⁻¹) in chloroform/1,2-dichlorobenzene (1:1 to 100:1, vol/vol) were thoroughly mixed and spin-cast on the top of the PEDOT:PSS layer. The thickness of MEH-PPV:TiO₂ nanorod film was 180 nm. Then, the 100 nm Al electrode was vacuum deposited on the hybrid layer.

By inserting the TiO₂ nanorod thin film between the MEH-PPV:TiO₂ nanorod hybrid and Al electrode, an improved device with a configuration of ITO/PEDOT:PSS/MEH-PPV:TiO₂ nanorods/TiO₂ nanorods/Al was made. The TiO₂

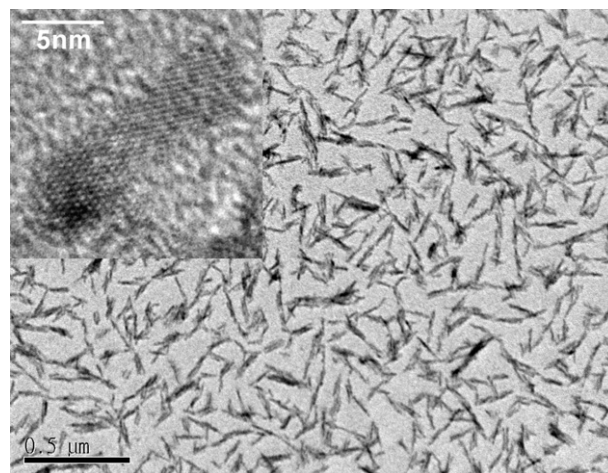


Figure 1. Anatase TiO₂ nanorod structure images observed by TEM and HRTEM (inset).

nanorods dissolved in chloroform:ethanol = 4:1 solution were spin-cast on the top of the MEH-PPV:TiO₂ nanorods hybrid to obtain a TiO₂ nanorod thin film of 70 nm thickness. In order to minimize the redissolving of MEH-PPV:TiO₂ layer, we have spin-coated concentrated nanorods solution (0.05 ml, 25 mg ml⁻¹) on the MEH-PPV:TiO₂ nanorod hybrid at very high speed (6000 rpm). An ITO/PEDOT:PSS/MEH-PPV:TiO₂ nanorods/MEH-PPV/Al photovoltaic device was fabricated as a reference. A 130 nm MEH-PPV layer on an MEH-PPV:TiO₂ nanorod hybrid was made by spin coating. The MEH-PPV in chloroform (20 mg ml⁻¹) solution was also spin-cast at a very high speed of 6000 rpm.

The crystalline structure of the nanorods was studied using x-ray diffraction (XRD) (Philips PW3040 with filtered Cu K α radiation ($\lambda = 1.54056 \text{ \AA}$)). The analysis of TiO₂ nanorods was performed using a JOEL JEM-1230 transmission electron microscope (TEM) operating at 120 keV or a 2000FX high resolution transmission electron microscope (HRTEM) at 200 keV. The film thickness was determined by an α -stepper (DEKTAK 6M 24383). The film morphology was observed by atomic force microscopy (AFM) (Digital Instruments Nanoscope III). The current–voltage (*I*–*V*) characterization (Keithley 2400 source meter) was performed under 10⁻³ Torr vacuum, with monochromatic illumination at a defined beam size (Oriel Inc.). The Air Mass (AM) 1.5 condition was measured using a calibrated solar simulator (Oriel Inc.) with irradiation intensity of 100 mW cm⁻². Once the power from the simulator was determined, a 400 nm cutoff filter was used to remove the UV light. The 80 nm MEH-PPV and MEH-PPV:TiO₂ films were cast on quartz substrate to obtain UV–Visible absorption (Jasco V-570) and photoluminescence (PL) (Perkin-Elmer FS-55) measurements.

3. Results and discussion

The TEM image of TiO₂ nanorods (figure 1) reveals that the TiO₂ nanorod dimension is 20–40 nm in length and 4–5 nm in diameter. The HRTEM image indicates that the TiO₂ nanorods had high crystallinity.

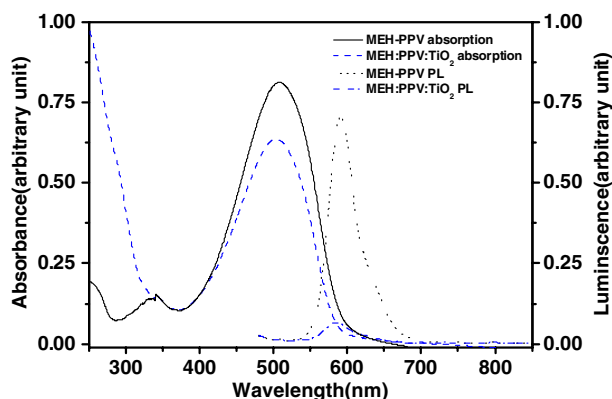


Figure 2. Absorption spectra of MEH-PPV films (solid line) and MEH-PPV:TiO₂ nanorod (52 wt%) hybrid (dashed line) of thickness 80 nm, and photoluminescence spectra of MEH-PPV films (dotted line) and MEH-PPV:TiO₂ nanorod (52 wt%) hybrid (dash-dotted line), excited at 450 nm.

Figure 2 shows the absorption and PL spectra of pristine MEH-PPV and MEH-PPV:TiO₂ nanorod hybrid films respectively. The optical density of the absorption spectrum in the hybrid increases with respect to the pristine polymer, and whose form is the result of contributions from each component. The absorption at wavelength less than 350 nm results mainly from the TiO₂ nanorods. In contrast, the yield of the PL emission decreases substantially, suggesting the occurrence of significant PL quenching in the hybrid [24]. Decreases in PL yield are attributed to the quenching of the MEH-PPV PL emission by the TiO₂ nanorods, acting as an electron accepting species, where significant charge separation takes place due to large interfacial areas for exciton dissociation.

As a starting point, we made a standard hybrid device structure similar to those previous reported polymer:nanocrystal photovoltaic devices, resulting in devices with external quantum efficiencies of the order up to 10%. A schematic diagram of our standard device configuration is shown in figure 3(a), which consists of a transparent indium–tin-oxide (ITO) conducting electrode, poly(3,4-ethylenedioxythiophene)–poly(styrenesulfonate) (PEDOT:PSS), the MEH-PPV:TiO₂ nanorod hybrid film, and an aluminium (Al) electrode. We have further modified the device configuration by including an additional electron conducting layer of TiO₂ nanorods sandwiched between the active layer and the aluminium electrode to improve device performance, as shown in figure 3(b).

We used tapping-mode AFM to investigate the structures and film morphology of these devices. Figure 4(a) shows the smooth topography of an MEH-PPV:TiO₂ nanorod hybrid with roughness 2 nm. The TiO₂ nanorods were randomly distributed in the polymer matrix for the interconnecting work formation. Figure 4(b) shows the phase image of an MEH-PPV:TiO₂ nanorod hybrid. Tapping-mode AFM can also give information about the materials at the film surface via phase images. Because a hard material generally shows a positive phase shift with respect to a soft material due to the cantilever oscillation being related to the power dissipated in a nonelastic tip–sample interaction [7], the bright areas in figure 4(b) are interpreted as the harder material of TiO₂ nanorods and the darker areas as the

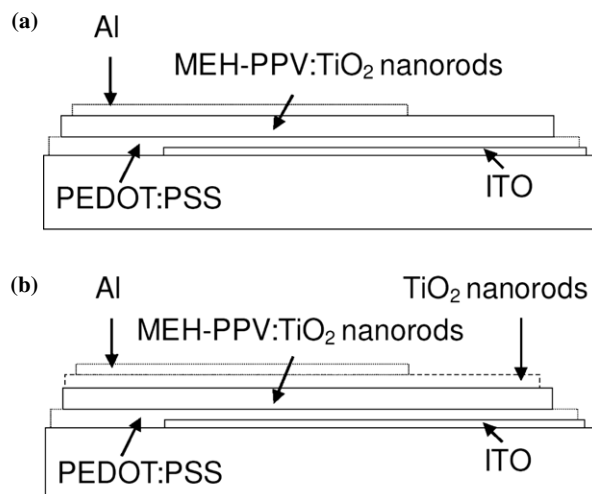


Figure 3. (a) The schematic structure of standard configuration MEH-PPV:TiO₂ nanorod hybrid photovoltaic devices. (b) Schematic structure of MEH-PPV:TiO₂ nanorod hybrid photovoltaic device included a TiO₂ nanorod layer.

soft material of polymer. A homogenous distribution of TiO₂ nanorods in polymer is observed in figure 4(b). Figure 4(c) shows the surface topography of a spin-cast TiO₂ nanorod layer on an MEH-PPV:TiO₂ nanorod hybrid. A feature of aggregation of nanorod structure was found. The TiO₂ nanorod thin film exhibits a porous structure of relatively high film roughness. Figure 4(d), the phase image of a TiO₂ nanorod thin film, shows a single phase of bright areas consisting of TiO₂ nanorods. The dark region in figure 4(d) could be seen as deep pores of the TiO₂ nanorod thin film, which is consistent with the surface topography observed in figure 4(b). From the results above, we have constructed an interconnecting network in an MEH-PPV:TiO₂ nanorod photoactive hybrid and a thin film composed of mere TiO₂ nanorods sandwiched between a hybrid layer and Al electrode through our process conditions.

An optimal composition between polymer and nanorods is required to achieve balanced exciton dissociation and charge transport. We investigated the effect of TiO₂ nanorod compositions on device performance. The best performance of this type of device was obtained at a concentration of MEH-PPV:TiO₂ (52 wt%). Lower power conversion efficiencies were obtained either at lower TiO₂ concentration (MEH-PPV:TiO₂ (40 wt%)) or higher concentration (MEH-PPV:TiO₂ (64 wt%)). This implies that, under those conditions, polymer–TiO₂ interfacial areas were not maximized for exciton dissociation or that the donor–acceptor interpenetrating networks formed cannot meet the requirements for the most efficient charge transport. We have varied the compositions of TiO₂ in the hybrid, the film thicknesses of the active layer and the types of solvent to achieve the optimal performance of the standard configuration device; however, the external quantum efficiency was limited to less than 10%.

Based upon considering the energy levels of the respective materials in the device, a TiO₂ nanorod layer inserted between the active layer and the aluminium electrode is appropriate for offering a better connectivity of electron transport path to

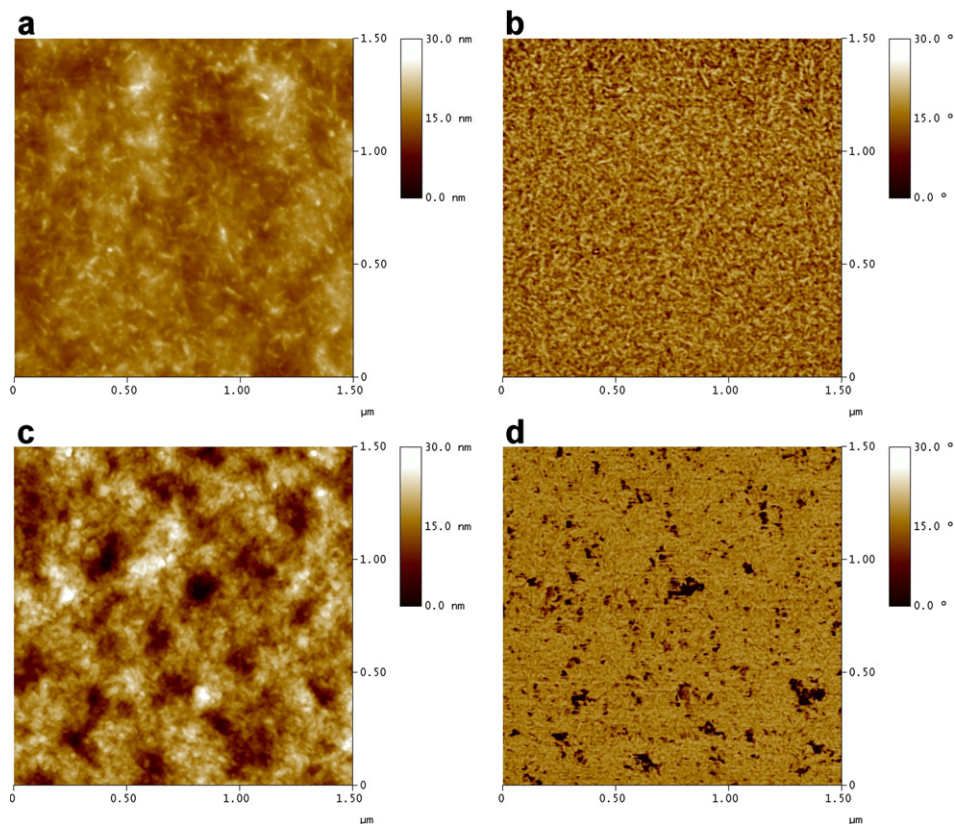


Figure 4. AFM images showing the surface morphology of an MEH-PPV:TiO₂ nanorod hybrid film and TiO₂ nanorod film. (a) Height image of spin-cast film of MEH-PPV:TiO₂ (52 wt%) nanorod hybrid. The image size is 1.5 μm × 1.5 μm, and the vertical scale is 30 nm. (b) Phase image of MEH-PPV:TiO₂ (52 wt%) nanorod hybrid film. The image size is 1.5 μm × 1.5 μm, and the vertical scale is 30°. (c) Height image of spin-cast film of TiO₂ nanorods on MEH-PPV:TiO₂ nanorod hybrid film. The image size is 1.5 μm × 1.5 μm, and the vertical scale is 30 nm. (d) Phase image of TiO₂ nanorod film on MEH-PPV:TiO₂ nanorod hybrid film. The image size is 1.5 μm × 1.5 μm, and the vertical scale is 30°.

the electrode. The functions of the TiO₂ nanorod layer can be explained by the band diagram in figure 5(a). The energy level diagram demonstrates that the TiO₂ nanorod layer acts as a hole-blocking electron-transporting layer in this device. As the electron–hole pairs are generated by incident light, an efficient charge separation occurs at the interface of the MEH-PPV:TiO₂ nanorod hybrid. Electrons move toward the aluminium electrode and holes move toward the ITO electrode. The addition of the continuous TiO₂ nanorod thin film allows for the current to be conducted effectively and also prevents electrons from back recombination with holes in the MEH-PPV. The TiO₂ nanorod layer acts as a hole-blocking layer because of lower valence band value. In contrast, on inserting a thin MEH-PPV layer instead, the device is energetically unfavorable for electron transport.

Figure 5(b) shows the current–voltage response of the devices with and without a TiO₂ nanorod layer. The device containing a TiO₂ nanorod layer increases the short-circuit current density by a factor of 2.5 with respect to a device without the layer. For a comparison, the thin TiO₂ nanorod layer was replaced with a thin MEH-PPV layer and a ~3 order of magnitude of decrease in the short-circuit current was found. Apart from the hole-blocking electron-transporting function of TiO₂ nanorod layer mentioned above, the interfaces introduced (MEH-PPV:TiO₂/TiO₂ and TiO₂/Al) seem more beneficial

to charge transport as compared to the MEH-PPV:TiO₂/Al contact. The TiO₂ nanorod layer can be connected to the TiO₂ nanorods in the active hybrid. In addition, the rough surface of the TiO₂ layer can lead to stronger contact and increased contact area to the Al electrode. Besides, inserting this layer can create a second interfacial area for exciton dissociation that might increase the charge transfer rate. To introduce an additional titanium oxide thin film as a hole-blocking electron-transporting layer through various approaches has been presented in producing higher efficiency heterojunction organic solar cells [14, 15, 25, 26]. Here we present a thin film of crystalline TiO₂ nanorods made via a fully solution process that can lead to improvement in device performance. The TiO₂ nanorod thin film could be explored as a promising hole-blocking electron-transporting layer in photovoltaic devices.

An equivalent circuit has frequently been used to describe the electric behaviour of a photovoltaic device [2]. We further analysed the characteristics of the devices based upon this equivalent circuit. The current density versus voltage characteristics can be described by the following equation:

$$I = I_0 \times \left[\exp\left(\frac{U - IR_S}{nkT}\right) - 1 \right] + \frac{U - IR_S}{R_{SH}} - I_{PH} \quad (1)$$

where I_0 is the saturation current, e is the magnitude of the electronic charge, U is the applied voltage, n is the

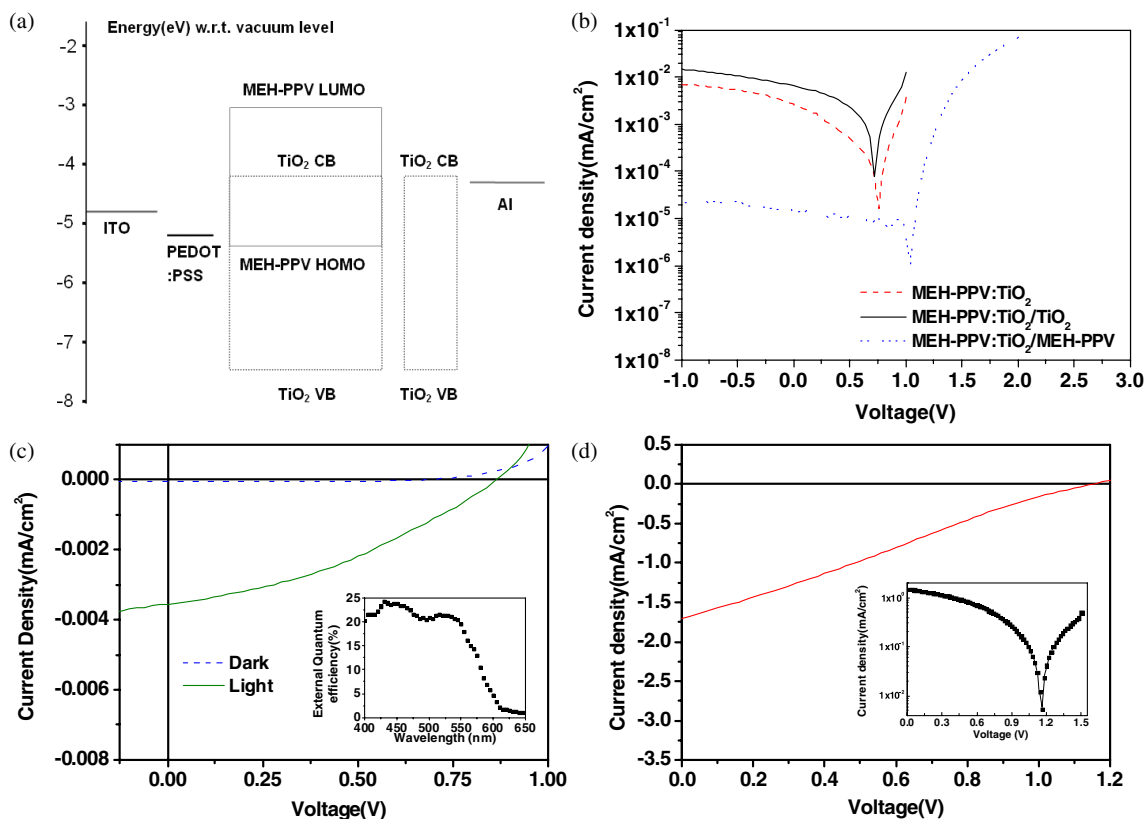


Figure 5. (a) Flat band energy-level diagram of ITO/PEDOT:PSS/MEH-PPV:TiO₂nanorods/TiO₂ nanorods/Al devices. (b) Plots of current density as the function of applied voltage for three different configuration devices under 0.09 mW cm⁻² illumination at 560 nm. (MEH-PPV:TiO₂ nanorods (52 wt%) (dashed line); MEH-PPV:TiO₂ nanorods (52 wt%)/TiO₂ nanorods (solid line) and MEH-PPV : TiO₂ nanorods (52 wt%)/MEH-PPV (dotted line)). (c) Plot of current density versus voltage in the dark (dashed line); and under 0.05 mW cm⁻² illumination at 565 nm (solid line, $V_{oc} = 0.86$ V, $J_{sc} = -0.0035$ mA cm⁻², FF = 0.35 and $\eta = 2.2\%$). The inset shows the external quantum efficiency versus wavelength of the device. The device structure is ITO/PEDOT:PSS/MEH-PPV:TiO₂ nanorods (52 wt%)/TiO₂ nanorods/Al. (d) The corresponding $I-V$ curve of the ITO/PEDOT:PSS/MEH-PPV:TiO₂ nanorods (52 wt%)/TiO₂ nanorods/Al device at AM 1.5 illumination (100 mW cm⁻²). ($V_{oc} = 1.15$ V, $J_{sc} = -1.7$ mA cm⁻², FF = 0.25 and $\eta = 0.49\%$). The logarithmic $I-V$ characteristic of the device is shown in the inset.

ideality factor, k is Boltzmann's constant, T is the absolute temperature, R_S is the series resistance, R_{SH} is the shunt resistance and I_{PH} is the photocurrent [2, 27]. The current-voltage characteristics are largely dependent on the series and shunt resistance. A lower series resistance means that higher current will flow through the device. High shunt resistance corresponds to fewer shorts or leaks in the device. The ideal cell would have a series resistance approaching zero and shunt resistance approaching infinity. The series resistance can be estimated from the inverse slope at a positive voltage where the $I-V$ curves become linear. The shunt resistance can be derived by taking the inverse slope of the $I-V$ curves around 0 V.

$$R_S = \lim_{V \rightarrow \infty} \left(\frac{dV}{dI} \right) \quad (2)$$

$$R_{SH} \approx \frac{dV}{dI} \quad (V = 0) \quad R_S \ll R_{SH}. \quad (3)$$

The R_S and R_{SH} were analysed from the $I-V$ curves of the devices (figure 5(b)); it is found that a significant, nearly 60%, reduction in R_S occurred as the TiO₂ nanorod layer was introduced into the device. A slight reduction of the shunt resistance was observed also. The series resistance can be

expressed as the sum of the bulk and interfacial resistance. It is likely that two interfaces that have been introduced (MEH-PPV:TiO₂/TiO₂ and TiO₂/Al) combined with the TiO₂ nanorod layer offer a much lower magnitude of series resistance as compared to the MEH-PPV:TiO₂/Al contact. The introducing of the TiO₂ layer decreases the series resistance in the device and thereby increases the current.

The performance of the device with a structure of ITO/PEDOT:PSS/MEH-PPV:TiO₂ nanorods (52 wt%)/TiO₂ nanorods/Al was evaluated. The $I-V$ characteristic of the device exhibits a short-circuit current density (J_{sc}) of -0.0035 mA cm⁻², an open circuit voltage (V_{oc}) of 0.86 V and a fill factor (FF) of 0.35. A power conversion efficiency (η) of 2.2% is achieved under 0.05 mW cm⁻² illumination at 565 nm (figure 5(c)). The inset shows the external quantum efficiency (EQE) of the device under illumination. A maximum EQE of 24% under 0.07 mW cm⁻² at 430 nm is achieved. Figure 5(d) presents the characteristics of the device tested under AM 1.5 illumination with an intensity of 100 mW cm⁻². The J_{sc} , FF, and V_{oc} are -1.7 mA cm⁻², 0.25, and 1.15 V, respectively for the device, yielding a power conversion efficiency of 0.49%. Work to optimize the device efficiency is still under way, to achieve better device efficiency.

4. Conclusions

In conclusion, we have used TiO₂ nanorods as efficient electron acceptors and transport components in the active layer of our hybrid organic photovoltaic device. A TiO₂ nanorod layer between the active layer and the electron-collecting electrode provides an enlarged interconnecting network for electrical transport near the aluminium electrode, leading to a 2.5-fold increase in the short-circuit current under illumination. These results suggest that one-dimensional TiO₂ nanorods are a promising material for hybrid organic solar cell applications. Further improvements in the device performance could be accomplished by controlling the nanorod sizes and by improving the polymer:TiO₂ nanorod interface.

Acknowledgments

The authors thank the National Science Council of the Republic of China (NSC94-2120-M-002-012) and the US Air Force Office of Scientific Research (AFOSR-AOARD-04-23) for financial support of this research. Thanks are also due to Mr An-Jey Su of the University of Pittsburgh for editing our manuscript.

References

- [1] Huynh W U, Dittmer J J and Alivisatos A P 2002 *Science* **295** 2425
- [2] Ma W, Yang C, Gong X, Lee K and Heeger A J 2005 *Adv. Funct. Mater.* **15** 1617
- [3] Shaheen S E, Brabec C J, Sariciftci N S, Padiner F, Fromherz T and Hummelen J C 2001 *Appl. Phys. Lett.* **78** 841
- [4] Yang X, Loos J, Veenstra S C, Verhees W J H, Wienk M M, Kroon J M, Michels M A J and Janssen R A J 2005 *Nano Lett.* **5** 579
- [5] Granström M, Petritsch K, Arias A C, Lux A, Andersson M R and Friend R H 1998 *Nature* **395** 257
- [6] Greenham N C, Peng X and Alivisatos A P 1996 *Phys. Rev. B* **54** 17628
- [7] Beek W J E, Wienk M M, Kemerink M, Yang X and Janssen R A J 2005 *J. Phys. Chem. B* **109** 9505
- [8] Kwong C Y, Choy W C H, Djurišić A B, Chui P C, Cheng K W and Chan W K 2004 *Nanotechnology* **15** 1156
- [9] Huynh W U, Dittmer J J, Libby W C, Whiting G L and Alivisatos A P 2003 *Adv. Funct. Mater.* **13** 73
- [10] Sun B, Marx E and Greenham N C 2003 *Nano Lett.* **3** 961
- [11] Jiu J, Isoda S, Wang F and Adachi M 2006 *J. Phys. Chem. B* **110** 2087
- [12] Breeze A J, Schlesinger Z, Carter S A and Brock P J 2001 *Phys. Rev. B* **64** 125205
- [13] Fan Q, McQuillin B, Bradley D D C, Whitelegg S and Seddon A B 2000 *Chem. Phys. Lett.* **347** 325
- [14] Wang H, Oey C C, Djurišić A B, Man K K Y, Chan W K, Xie M H, Leung Y H, Chui P C, Pandey A and Nunzi J-M 2005 *Appl. Phys. Lett.* **87** 023507
- [15] Oey C C, Djurišić A B, Wang H, Man K K Y, Chan W K, Xie M H, Leung Y H, Pandey A, Nunzi J-M and Chui P C 2006 *Nanotechnology* **17** 706
- [16] Ravirajan R, Bradley D D C, Nelson J, Haque S A, Durrant J R, Smith H J P and Kroon J M 2005 *Appl. Phys. Lett.* **86** 143101
- [17] Van Hal P A, Wienk M M, Kroon J M, Verhees W J, Sloof L H, Van Gennip W J H, Jonkheijm P and Janssen R A J 2003 *Adv. Mater.* **15** 118
- [18] Coakley K M and McGehee M D 2003 *Appl. Phys. Lett.* **83** 3380
- [19] Liu Y, Summers M A, Edler C, Fréchet J M J and McGehee M D 2005 *Adv. Mater.* **17** 2960
- [20] Qiao Q and McLeskey J T 2005 *Appl. Phys. Lett.* **86** 153501
- [21] Petrella A, Tamborra M, Cozzoli P D, Curri M L, Striccoli M, Cosma P, Farinola G M, Babudri F, Naso F and Agostiano A 2004 *Thin Solid Films* **451/452** 64
- [22] Petrella A, Tamborra M, Curri M L, Cosma P, Striccoli M, Cozzoli P D and Agostiano A 2005 *J. Phys. Chem. B* **109** 1554
- [23] Cozzoli P D, Kornowski A and Weller H 2003 *J. Am. Chem. Soc.* **125** 14539
- [24] Lin Y Y, Chen C W, Chang J, Lin T Y, Liu I S and Su W F 2006 *Nanotechnology* **17** 1260
- [25] Thelakatt M, Schmitz C and Schmidt H-W 2002 *Adv. Mater.* **14** 577
- [26] Kim J Y, Kim S H, Lee H-H, Lee K, Ma W, Gong X and Heeger A J 2006 *Adv. Mater.* **18** 572
- [27] Watt A A R, Blake D, Warner J H, Thomsen E A, Tavenner E L, Rubinsztein-Dunlop H and Meredith P 2005 *J. Phys. D: Appl. Phys.* **38** 2006